PHARMACIA

Pharmacia 73: e194529
DOI 10.3897/pharmacia.73.e194529

Research Article

Design, synthesis, antioxidant activity, SAR, molecular docking, and ADME studies of novel hydroxyl-derived compounds

Emilio Mateev[1], Diana Tzankova[1], Valentin Karatchobanov[1], Ali Irfan[2], Eva-Maria Pepeldzhiyska[1], Stefan Kostov[1], Alexander Zlatkov[1]

1 *Department of Pharmaceutical Chemistry, Faculty of Pharmacy, Medical University–Sofia, 2 Dunav str., 1000 Sofia, Bulgaria*
2 *The Green Institute of Chemical, Biomedical and Environmental Sciences (GICBES), Lahore, 54000, Pakistan*

Corresponding author: Emilio Mateev (e.mateev@pharmfac.mu-sofia.bg)

Received 6 April 2026 ♦ **Accepted** 27 April 2026 ♦ **Published** 29 July 2026

Citation: Mateev E, Tzankova D, Karatchobanov V, Irfan A, Pepeldzhiyska E-M, Kostov S, Zlatkov A (2026) Design, synthesis, antioxidant activity, SAR, molecular docking, and ADME studies of novel hydroxyl-derived compounds. Pharmacia 73: e194529. https://doi.org/10.3897/pharmacia.73.e194529

Abstract

Twenty novel pyrrole-based hydrazide-hydrazone derivatives (GlyOH1-4, BAlaOH1-4, IleOH1-4, PheOH1-4, TrpOH1-4), bearing hydroxyl-substituted aromatic aldehydes and diverse amino acid scaffolds, were designed, synthesized in 83-95% yields, and fully characterized by FT-IR, ^{1}H-NMR and ^{13}C-NMR. All compounds exhibited radical-scavenging activity in DPPH and ABTS assays, with TrpOH-3 emerging as the lead (IC_{50} 3.96 ± 0.20 μM ABTS, 9.17 ± 0.09 μM DPPH), outperforming Trolox in both. SAR analysis revealed optimal activity from tryptophan scaffolds and catechol-like (2,3,4- or 2,4,5-trihydroxy) moieties, attributed to enhanced HAT/SET mechanisms and radical stabilization. Molecular docking of TrpOH-3 to Keap1 Kelch domain (PDB: 4L7B) yielded -6.25 kcal/mol, featuring H-bonds (Ser602, Ser363, Tyr525), water-mediated interactions, and Br-Tyr334 halogen bonding, supporting Nrf2 activation potential. ADME predictions indicated drug-likeness (1 Ro5 violation), though high MW limited CNS permeability. These multifunctional antioxidants hold promise for oxidative stress-related disorders.

Keywords

Hydrazide-hydrazones; antioxidants; molecular docking; SAR

Introduction

The balance between endogenous antioxidant systems and reactive oxygen species (ROS) generated during normal cellular metabolism is crucial for maintaining cellular homeostasis. Mitochondria, as the primary site of ROS production during oxidative phosphorylation, contribute significantly to this balance. Electron leakage from the electron transport chain generates superoxide radicals that can damage other species. Disruptions in this equilibrium lead to oxidative stress, characterized by excessive ROS accumulation, which impairs cellular function and promotes macromolecular damage (Kowalczyk et al. 2021).

Elevated ROS concentrations, particularly those originating from mitochondria, disrupt this balance and initiate oxidative stress that damages lipids, proteins, DNA, and other biomolecules in living cells. This arises from ROS-mediated peroxidation, oxidation, and strand breaks, compromising membrane integrity, enzyme function, and

Copyright *Mateev E et al.* This is an open access article distributed under the terms of the Creative Commons Attribution License (CC-BY 4.0), which permits unrestricted use, distribution, and reproduction in any medium, provided the original author and source are credited.

PENSOFT

genomic stability. Consequently, chronic oxidative stress contributes to a wide array of pathophysiological conditions (Nakai and Tsuruta 2021).

Key ROS include oxygen-centered free radicals such as superoxide anion (O_2-), hydroperoxyl (HO_2-), peroxyl (ROO-), alkoxyl (RO-), hydroxyl (HO-), and nitric oxide (NO-), alongside non-radical species like hydrogen peroxide (H_2O_2). These species vary in reactivity and lifetime, with the hydroxyl radical being highly destructive due to its non-specific reactivity with nearby biomolecules. Mitochondria primarily produce superoxide via complexes I and III, which dismutates to H_2O_2 and can further form more potent radicals (Korovesis et al. 2023).

Moreover, excessive ROS production has been strongly implicated in aging through the accumulation of oxidative damage and mitochondrial dysfunction, as well as in metabolic disorders like obesity (via adipocyte inflammation), psychiatric conditions such as depression (through neuroinflammation), ocular pathologies including cataracts (lens protein oxidation), carcinogenesis (DNA mutagenesis), and the pathogenesis of neurodegenerative diseases like Alzheimer's and Parkinson's (protein aggregation and neuronal loss). These links highlight ROS as a common mechanistic thread across diverse diseases (Leyane et al. 2022).

Schiff bases, characterized by the azomethine (-CH=N-) linkage formed through facile condensation of aldehydes or ketones with primary amines, represent privileged scaffolds in medicinal chemistry owing to their structural versatility, ease of synthesis, and inherent pharmacological profiles. The imine (C=N) functionality promotes extended π-conjugation and electron delocalization, facilitating efficient radical stabilization and quenching, often synergistically amplified by proximal phenolic hydroxyl groups that enable hydrogen atom transfer (HAT) or single electron transfer (SET) mechanisms. These properties confer superior ROS-scavenging potency relative to precursor carbonyl compounds, complemented by metal-chelating ability that sequesters pro-oxidant transition metals (e.g., Fe^{2+}, Cu^{2+}), mitigating Fenton-type reactions (Rana et al. 2024).

SAR studies consistently reveal that electron-donating substituents (e.g., hydroxyl at ortho/para positions, methoxy) on aromatic rings enhance antioxidant activity by lowering bond dissociation enthalpy (BDE) of phenolic O-H bonds and elevating HOMO energies for better electron donation, as validated by DPPH/ABTS assays. Conversely, electron-withdrawing groups diminish efficacy, underscoring the role of resonance stabilization in phenoxyl radical intermediates. Their biocompatibility and low toxicity further position Schiff bases as attractive alternatives to synthetic antioxidants like BHT, with metal complexes often exhibiting augmented activity via cooperative ligand-metal redox cycling (Rana et al. 2024).

Recent investigations affirm their therapeutic promise against oxidative stress-driven disorders, including neurodegeneration and inflammation, where *in silico* tools like DFT (for BDE, ionization potentials), molecular docking (to antioxidant enzymes like MPO or Keap1), and ADME predictions have streamlined lead optimization. This multifaceted evaluation—bridging synthesis, bioassays, SAR, computation, and pharmacokinetics—enables rational design of multifunctional antioxidants with enhanced potency and translational potential, as exemplified by hydroxyl-substituted derivatives outperforming standards in preclinical models (Abdullah et al. 2026).

Therefore, the present study aimed to design and synthesize a series of 20 novel hydrazide-hydrazone derivatives featuring hydroxyl moieties and diverse aromatic side chains to explore their antioxidant potential. These compounds were evaluated for radical scavenging efficacy using DPPH and ABTS assays, complemented by comprehensive SAR analysis to delineate structural prerequisites for activity. Additionally, molecular docking studies against key oxidative stress targets (e.g., MPO, Keap1-Nrf2) alongside DFT computations and ADME predictions offer mechanistic insights and guide future lead optimization for therapeutic applications.

Materials and methods

Synthesis

All solvents and reagents employed in the experiments were purchased from Sigma-Aldrich (St. Louis, MO, USA) and used without additional purification. Reaction monitoring was performed by thin-layer chromatography (TLC) on silica gel-coated aluminum plates, employing a chloroform-ethanol (1:0.8) mobile phase. Melting points were measured using a Kruss M5000 apparatus (KRÜSS, Hamburg, Germany). Infrared spectra (4000-400 cm^{-1}) were acquired on a Nicolet iS10 FT-IR spectrometer (Thermo Fisher Scientific, MA, USA) equipped with a Smart iTR accessory. ^{1}H-NMR spectra were recorded at 400 MHz on a Bruker Avance Neo spectrometer (Biospin GmbH, Baden-Württemberg, Germany) with tetramethylsilane (TMS) as the internal standard.

The novel hydrazide-hydrazones (GlyOH1-4, BAlaOH1-4, IleOH1-4, PheOH1-4, TrpOH1-4) were synthesized by condensing equimolar amounts (0.1 mol) of the corresponding amino acid hydrazides with aldehydes 1-4 (0.12 mol) in a minimal volume of glacial acetic acid. The hydrazide was initially dissolved in acetic acid at room temperature, followed by addition of the aldehyde derivative, and the reaction mixture was refluxed for 1 hr to afford the target compounds in 82-95% yield after recrystallization from ethanol.

ethyl 5-(4-bromophenyl)-1-(2-(2-(2,4-dihydroxybenzylidene)hydrazinyl)-2-oxoethyl)-2-methyl-1H-pyrrole-3-carboxylate (GlyOH-1)

Solid; Yield 95%; Melting point 168.1 °C; IR *ν*max: 3359 cm^{-1} (O-H broad), 3275 cm^{-1} (N–H stretch), 1720 cm^{-1} (C=O stretch), 1668 cm^{-1} (C=N imine); ^{1}H NMR (DMSO, 400 MHz): δ 1.30 [t, 3H, OCH_2CH_3], 2.47 [s, 3H, CH_3], 4.29 [q, 2H, OCH_2CH_3], 4.74 [s, 2H,

NCH_2CO], 6.33 [d, 1H, Ar–H], 6.75 [s, 1H, pyrrole-H], 7.52 [d, 1H, Ar–H], 7.54 [d, 1H, Ar–H], 7.55 [d, 2H, Ar–H], 7.55 [d, 2H, Ar–H], 7.78 [d, 2H, Ar–H], 7.78 [d, 2H, Ar–H], 8.74 [s, 1H, N=CH], 10.10 [s, 1H, Ar–OH], 11.07 [s, 1H, CONH], 11.68 [s, 1H, Ar–OH]; ^{13}C NMR (100 MHz, DMSO): δ 11.5, 14.1, 38.3, 60.9, 103.7, 104.7, 108.2, 108.6, 111.1, 123.1, 128.3 (2C). 132.0, 132.1 (2C), 132.7, 133.8, 142.1, 146.0, 162.2, 162.5, 165.9 and 171.0;

ethyl 5-(4-bromophenyl)-2-methyl-1-(2-oxo-2-(2-(2,3,4 trihydroxybenzylidene)hydrazinyl) ethyl)-1H-pyrrole-3-carboxylate (GlyOH-2)

Solid; Yield 93%; Melting point 172.3 °C; IR *ν*max: 3322 cm^{-1} (O-H broad), 3268 cm^{-1} (N–H stretch), 1718 cm^{-1} (C=O stretch), 1665 cm^{-1} (C=N imine); ^{1}H NMR (DMSO, 400 MHz): δ 1.30 [t, 3H, OCH_2CH_3], 2.47 [s, 3H, CH_3], 4.29 [q, 2H, OCH_2CH_3], 4.74 [s, 2H, NCH_2CO], 6.27 [d, 1H, Ar–H], 6.75 [s, 1H, pyrrole-H], 7.10 [d, 1H, Ar–H], 7.55 [d, 2H, Ar–H], 7.55 [d, 2H, Ar–H], 7.78 [d, 2H, Ar–H], 7.78 [d, 2H, Ar–H], 8.73 [s, 1H, Ar–OH], 8.74 [s, 1H, N=CH], 9.48 [s, 1H, Ar–OH], 11.07 [s, 1H, CONH], 13.78 [s, 1H, Ar–OH]; ^{13}C NMR (100 MHz, DMSO): δ 11.5, 14.1, 38.3, 60.9, 104.7, 108.2, 110.0, 112.5, 123.1, 126.4, 128.3 (2C), 132.0, 132.1 (2C), 132.7, 136.1, 142.1, 146.0, 152.4, 153.1, 165.9 and 171.1;

ethyl 5-(4-bromophenyl)-2-methyl-1-(2-oxo-2-(2-(2,4,5-trihydroxybenzylidene)hydrazinyl) ethyl)-1H-pyrrole-3-carboxylate (GlyOH-3)

Solid; Yield 92%; Melting point 212.6 °C; IR *ν*max: 3383 cm^{-1} (O-H broad), 3280 cm^{-1} (N–H stretch), 1722 cm^{-1} (C=O stretch), 1672 cm^{-1} (C=N imine); ^{1}H NMR (δH, 400 MHz, DMSO): δ 1.30 [t, 3H, OCH_2CH_3], 2.47 [s, 3H, CH_3], 4.29 [q, 2H, OCH_2CH_3], 4.74 [s, 2H, NCH_2CO], 6.15 [d, 1H, Ar–H], 6.75 [s, 1H, pyrrole-H], 6.91 [d, 1H, Ar–H], 7.55 [d, 2H, Ar–H], 7.55 [d, 2H, Ar–H], 7.78 [d, 2H, Ar–H], 7.78 [d, 2H, Ar–H], 8.74 [s, 1H, N=CH], 9.48 [s, 1H, Ar–OH], 9.48 [s, 1H, Ar–OH], 11.07 [s, 1H, CONH], 11.68 [s, 1H, Ar–OH]; ^{13}C NMR (100 MHz, DMSO): δ 11.5, 14.1, 38.3, 60.9, 104.7, 105.1, 108.2, 112.5, 117.7, 123.1, 128.3 (2C), 132.0, 132.1 (2C), 132.7, 138.7, 142.1, 146.0, 152.4, 155.1, 165.9 and 171.0;

ethyl 5-(4-bromophenyl)-2-methyl-1-(2-oxo-2-(2-(2,4,6-trihydroxybenzylidene)hydrazinyl) ethyl)-1H-pyrrole-3-carboxylate (GlyOH-4)

Solid; Yield 93%; Melting point 198.1 °C; IR *ν*max: 3402 cm^{-1} (O-H broad), 3265 cm^{-1} (N–H stretch), 1715 cm^{-1} (C=O stretch), 1670 cm^{-1} (C=N imine); ^{1}H NMR (δH, 400 MHz, DMSO): δ 1.30 [t, 3H, OCH_2CH_3], 2.47 [s, 3H, CH_3], 4.29 [q, 2H, OCH_2CH_3], 4.74 [s, 2H, NCH_2CO], 6.75 [s, 1H, pyrrole-H], 7.08 [d, 1H, Ar-H], 7.08 [d, 1H, Ar-H], 7.55 [d, 2H, Ar–H], 7.55 [d, 2H, Ar–H], 7.78 [d, 2H, Ar–H], 7.78 [d, 2H, Ar–H], 8.39 [s, 1H, N=CH], 10.27 [s, 1H, Ar–OH], 10.27 [s, 1H, Ar–OH], 10.40 [s, 1H, Ar–OH], 11.07 [s, 1H, CONH]; ^{13}C NMR (100 MHz, DMSO): δ 11.5, 14.1, 38.3, 60.9, 96.3 (2C), 104.7, 106.2, 108.2, 123.1, 128.3 (2C), 132.0, 132.1 (2C), 132.7, 142.1, 143.3, 163.6, 163.9 (2C), 165.9 and 171.0;

ethyl 5-(4-bromophenyl)-1-(3-(2-(2,4-dihydroxybenzylidene)hydrazinyl)-3-oxopropyl)-2-methyl-1H-pyrrole-3-carboxylate (BAlaOH-1)

Solid; Yield 92%; Melting point 173.6 °C; IR *ν*max: 3404 cm^{-1} (O-H broad), 3270 cm^{-1} (N–H stretch), 1716 cm^{-1} (C=O stretch), 1662 cm^{-1} (C=N imine); ^{1}H NMR (δH, 400 MHz, DMSO): δ 1.30 [t, 3H, OCH_2CH_3], 2.45 [t, 2H, CH_2CO], 2.47 [s, 3H, CH_3], 4.13 [t, 2H, NCH_2], 4.29 [q, 2H, OCH_2CH_3], 6.33 [d, 1H, Ar–H], 6.78 [s, 1H, pyrrole–H], 7.52 [d, 1H, Ar–H], 7.54 [d, 1H, Ar–H], 7.55 [d, 2H, Ar–H], 7.55 [d, 2H, Ar–H], 7.78 [d, 2H, Ar–H], 7.78 [d, 2H, Ar–H], 8.74 [s, 1H, N=CH], 10.10 [s, 1H, Ar–OH], 11.07 [s, 1H, CONH], 11.68 [s, 1H, Ar–OH]; ^{13}C NMR (100 MHz, DMSOd6): δ 11.8, 14.1, 36.8, 60.9, 103.7, 104.7, 108.2, 108.6, 111.1, 123.1, 128.3 (2C), 132.0, 132.1 (2C), 132.7, 133.8 , 142.1, 146.0, 162.2, 162.5, 165.9 and 167.7;

ethyl 5-(4-bromophenyl)-2-methyl-1-(3-oxo-3-(2-(2,3,4-trihydroxybenzylidene)hydrazinyl) propyl)-1H-pyrrole-3-carboxylate (BAlaOH-2)

Solid; Yield 93%; Melting point 181.2 °C; IR *ν*max: 3327 cm^{-1} (O-H broad), 3258 cm^{-1} (N–H stretch), 1714 cm^{-1} (C=O stretch), 1660 cm^{-1} (C=N imine); ^{1}H NMR (δH, 400 MHz, DMSOd6): δ 1.30 [t, 3H, OCH_2CH_3], 2.45 [t, 2H, CH_2CO], 2.47 [s, 3H, CH_3], 4.13 [t, 2H, NCH_2], 4.29 [q, 2H, OCH_2CH_3], 6.27 [d, 1H, Ar–H], 6.78 [s, 1H, pyrrole–H], 7.10 [d, 1H, Ar–H], 7.55 [d, 2H, Ar–H], 7.55 [d, 2H, Ar–H], 7.78 [d, 2H, Ar–H], 7.78 [d, 2H, Ar–H], 8.73 [s, 1H, Ar–OH], 8.74 [s, 1H, N=CH], 9.48 [s, 1H, Ar–OH], 11.07 [s, 1H, CONH], 13.78 [s, 1H, Ar–OH]; ^{13}C NMR (100 MHz, DMSO): δ 11.8, 14.1, 36.8, 60.9, 104.7, 108.2, 110.0, 112.5, 123.1, 126.4, 128.3 (2C), 132.0, 132.1 (2C), 132.7, 136.1, 142.1, 146.0, 152.4, 153.1, 165.9 and 167.7;

ethyl 5-(4-bromophenyl)-2-methyl-1-(3-oxo-3-(2-(2,4,5-trihydroxybenzylidene)hydrazinyl) propyl)-1H-pyrrole-3-carboxylate (BAlaOH-3)

Solid; Yield 93%; Melting point 219.2 °C; IR *ν*max: 3421 cm^{-1} (O-H broad), 3278 cm^{-1} (N–H stretch), 1720 cm^{-1} (C=O stretch), 1668 cm^{-1} (C=N imine); ^{1}H NMR (δH, 400 MHz, DMSO): δ 1.30 [t, 3H, OCH_2CH_3], 2.45 [t, 2H, CH_2CO], 2.47 [s, 3H, CH_3], 4.13 [t, 2H, NCH_2], 4.29 [q, 2H, OCH_2CH_3], 6.15 [d, 1H, Ar–H], 6.78 [s, 1H, pyrrole-H], 6.91 [d, 1H, Ar–H], 7.55 [d, 2H, Ar–H], 7.55 [d, 2H, Ar–H], 7.78 [d, 2H, Ar–H], 7.78 [d, 2H, Ar–H], 8.74 [s, 1H, N=CH], 9.48 [s, 1H, Ar–OH], 9.48 [s, 1H, Ar–OH], 11.07 [s, 1H, CONH], 11.68 [s, 1H, Ar–OH]; ^{13}C NMR (100 MHz, DMSOd6): δ 11.8, 14.1, 36.8, 60.9, 104.7, 105.1, 108.2, 112.5, 117.7, 123.1, 128.3 (2C), 132.0, 132.1 (2C), 132.7, 138.7, 142.1, 146.0, 152.4, 155.1, 165.9 and 167.7;

ethyl 5-(4-bromophenyl)-2-methyl-1-(3-oxo-3-(2-(2,4,6-trihydroxybenzylidene)hydrazinyl) propyl)-1H-pyrrole-3-carboxylate (BalaOH-4)

Solid; Yield 92%; Melting point 182.1 °C; IR *ν*max: 3404 cm^{-1} (O-H broad), 3262 cm^{-1} (N–H stretch), 1712 cm^{-1} (C=O stretch), 1665 cm^{-1} (C=N imine); ^{1}H NMR (δH, 400 MHz, DMSO): δ 1.30 [t, 3H, OCH_2CH_3], 2.45 [t, 2H, CH_2CO], 2.47 [s, 3H, CH_3], 4.13 [t, 2H, NCH_2], 4.29 [q, 2H, OCH_2CH_3], 6.78 [s, 1H, pyrrole-H], 7.08 [d, 1H, Ar-H], 7.08 [d, 1H, Ar-H], 7.55 [d, 2H, Ar–H], 7.55 [d, 2H, Ar–H], 7.78 [d, 2H, Ar–H], 7.78 [d, 2H, Ar–H], 8.39 [s, 1H, N=CH], 10.27 [s, 1H, Ar–OH], 10.27 [s, 1H, Ar–OH], 10.40 [s, 1H, Ar–OH], 11.07 [s, 1H, CONH]; ^{13}C NMR (100 MHz, DMSO): δ 11.8, 14.1, 36.8, 60.9, 96.3 (2C), 104.7, 106.2, 108.2, 123.1, 128.3 (2C), 132.0, 132.1 (2C), 132.7, 142.1, 143.3, 163.6, 163.9 (2C), 165.9 and 167.7;

ethyl 5-(4-bromophenyl)-1-(1-(2-(2,4-dihydroxybenzylidene)hydrazinyl)-3-methyl-1-oxopentan-2-yl)-2-methyl-1H-pyrrole-3-carboxylate (IleOH-1)

Solid; Yield 87%; Melting point 181.5 °C; IR *ν*max: 3401 cm^{-1} (O-H broad), 3285 cm^{-1} (N–H stretch), 1725 cm^{-1} (C=O stretch), 1675 cm^{-1} (C=N imine); ^{1}H NMR (δH, 400 MHz, DMSOd6): δ 0.93 [d, 3H, Ile-CH_3], 0.99 [d, 3H, Ile-CH_3], 1.30 [t, 3H, OCH_2CH_3], 1.55 [m, 2H, Ile-CH_2], 1.8 [m, 1H, Ile-CH], 2.47 [s, 3H, CH_3], 4.29 [q, 2H, OCH_2CH_3], 4.44 [t, 1H, Ile-α-CH], 6.33 [d, 1H, Ar–H], 6.78 [s, 1H, pyrrole–H], 7.52 [d, 1H, Ar–H], 7.54 [d, 1H, Ar–H], 7.55 [d, 2H, Ar–H], 7.55 [d, 2H, Ar–H], 7.78 [d, 2H, Ar–H], 7.78 [d, 2H, Ar–H], 8.74 [s, 1H, N=CH], 10.10 [s, 1H, Ar–OH], 11.07 [br s, 1H, CONH], 11.68 [s, 1H, Ar–OH]; ^{13}C NMR (100 MHz, DMSOd6): δ 11.3, 11.8, 14.1, 16.3, 26.4, 33.1, 60.9, 73.9, 103.7, 104.7, 108.2, 108.6, 111.1, 123.1, 128.3 (2C), 132.0, 132.1 (2C), 132.7, 133.8, 142.1, 146.0, 162.2, 162.5, 165.9 and 174.8;

ethyl 5-(4-bromophenyl)-2-methyl-1-(3-methyl-1-oxo-1-(2-(2,3,4-trihydroxybenzylidene) hydrazinyl)pentan-2-yl)-1H-pyrrole-3-carboxylate (IleOH-2)

Solid; Yield 86%; Melting point 189.7 °C; IR *ν*max: 3421 cm^{-1} (O-H broad), 3278 cm^{-1} (N–H stretch), 1723 cm^{-1} (C=O stretch), 1672 cm^{-1} (C=N imine); ^{1}H NMR (δH, 400 MHz, DMSOd6): δ 0.93 [d, 3H, Ile-CH_3], 0.99 [d, 3H, Ile-CH_3], 1.30 [t, 3H, OCH_2CH_3], 1.55 [m, 2H, Ile-CH_2], 1.8 [m, 1H, Ile-CH], 2.47 [s, 3H, CH_3], 4.29 [q, 2H, OCH_2CH_3], 4.44 [t, 1H, Ile-α-CH], 6.27 [d, 1H, Ar–H], 6.78 [s, 1H, pyrrole-H], 7.10 [d, 1H, Ar–H], 7.55 [d, 2H, Ar–H], 7.55 [d, 2H, Ar–H], 7.78 [d, 2H, Ar–H], 7.78 [d, 2H, Ar–H], 8.73 [s, 1H, Ar–OH], 8.74 [s, 1H, N=CH], 9.48 [s, 1H, Ar–OH], 11.07 [br s, 1H, CONH], 13.78 [s, 1H, Ar–OH]; ^{13}C NMR (100 MHz, DMSOd6): δ 11.3, 11.8, 14.1, 16.3, 26.4, 33.1, 60.9, 73.9, 104.7, 108.2, 110.0, 112.5, 123.1, 126.4, 128.3 (2C), 132.0, 132.1 (2C), 132.7, 136.1, 142.1, 146.0, 152.4, 153.1, 165.9 and 174.8;

ethyl 5-(4-bromophenyl)-2-methyl-1-(3-methyl-1-oxo-1-(2-(2,4,5-trihydroxybenzylidene) hydrazinyl)pentan-2-yl)-1H-pyrrole-3-carboxylate (IleOH-3)

Solid; Yield 89%; Melting point 226.5 °C; IR *ν*max: 3401 cm^{-1} (O-H broad), 3282 cm^{-1} (N–H stretch), 1728 cm^{-1} (C=O stretch), 1678 cm^{-1} (C=N imine); 1H NMR (δH, 400 MHz, DMSO): δ 0.93 [d, 3H, Ile-CH_3], 0.99 [d, 3H, Ile-CH_3], 1.30 [t, 3H, OCH_2CH_3], 1.55 [m, 2H, Ile-CH_2], 1.8 [m, 1H, Ile-CH], 2.47 [s, 3H, CH_3], 4.29 [q, 2H, OCH_2CH_3], 4.44 [t, 1H, Ile-α-CH], 6.15 [d, 1H, Ar–H], 6.78 [s, 1H, pyrrole-H], 6.91 [d, 1H, Ar–H], 7.55 [d, 2H, Ar–H], 7.55 [d, 2H, Ar–H], 7.78 [d, 2H, Ar–H], 7.78 [d, 2H, Ar–H], 8.74 [s, 1H, N=CH], 9.48 [s, 1H, Ar–OH], 9.48 [s, 1H, Ar–OH], 11.07 [br s, 1H, CONH], 11.68 [s, 1H, Ar–OH]; ^{13}C NMR (100 MHz, DMSOd6): δ 11.3, 11.8, 14.1, 16.3, 26.4, 33.1, 60.9, 73.9, 104.7, 105.1, 108.2, 112.5, 117.7, 123.1, 128.3 (2C), 132.0, 132.1 (2C), 132.7, 138.7, 142.1, 146.0, 152.4, 155.1, 165.9 and 174.8;

ethyl 5-(4-bromophenyl)-2-methyl-1-(3-methyl-1-oxo-1-(2-(2,4,6-trihydroxybenzylidene) hydrazinyl)pentan-2-yl)-1H-pyrrole-3-carboxylate (IleOH-4)

Solid; Yield 91%; Melting point 208.5 °C; IR *ν*max: 3421 cm^{-1} (O-H broad), 3275 cm^{-1} (N–H stretch), 1726 cm^{-1} (C=O stretch), 1676 cm^{-1} (C=N imine); 1H NMR (δH, 400 MHz, DMSO): δ 0.93 [d, 3H, Ile-CH_3], 0.99 [d, 3H, Ile-CH_3], 1.30 [t, 3H, OCH_2CH_3], 1.55 [m, 2H, Ile-CH_2], 1.8 [m, 1H, Ile-CH], 2.47 [s, 3H, CH_3], 4.29 [q, 2H, OCH_2CH_3], 4.44 [t, 1H, Ile-α-CH], 6.78 [s, 1H, pyrrole-H], 7.08 [d, 1H, Ar-H], 7.08 [d, 1H, Ar-H], 7.55 [d, 2H, Ar–H], 7.55 [d, 2H, Ar–H], 7.78 [d, 2H, Ar–H], 7.78 [d, 2H, Ar–H], 8.39 [s, 1H, N=CH], 10.27 [s, 1H, Ar–OH], 10.27 [s, 1H, Ar–OH], 10.40 [s, 1H, Ar–OH], 11.07 [br s, 1H, CONH]; ^{13}C NMR (100 MHz, DMSOd6): δ 11.3, 11.8, 14.1, 16.3, 26.4, 33.1, 60.9, 73.9, 96.3 (2C), 104.7, 106.2, 108.2, 123.1, 128.3 (2C), 132.0, 132.1 (2C), 132.7, 142.1, 143.3, 163.6, 163.9 (2C), 165.9 and 174.8;

ethyl 5-(4-bromophenyl)-1-(1-(2-(2,4-dihydroxybenzylidene)hydrazinyl)-1-oxo-3-phenylpropan-2-yl)-2-methyl-1H-pyrrole-3-carboxylate (PheOH-1)

Solid; Yield 86%; Melting point 191.4 °C; IR *ν*max: 3432 cm^{-1} (O-H broad), 3272 cm^{-1} (N–H stretch), 1715 cm^{-1} (C=O stretch), 1670 cm^{-1} (C=N imine); ^{1}H NMR (δH, 400 MHz, DMSOd6): δ 1.30 [t, 3H, OCH_2CH_3], 2.47 [s, 3H, CH_3], 2.94-3.19 [m, 2H, Phe-CH_2], 4.29 [q, 2H, OCH_2CH_3], 5.02 [t, 1H, Phe-α-CH], 6.33 [d, 1H, Ar-H], 6.78 [s, 1H, pyrrole-H], 7.19 [t, 1H, Ar-H], 7.21 [t, 1H, Ar-H], 7.21 [t, 1H, Ar-H], 7.23 [t, 1H, Ar-H], 7.23 [t, 1H, Ar-H], 7.52 [d, 1H, Ar–H], 7.54 [d, 1H, Ar–H], 7.55 [d, 2H, Ar–H], 7.55 [d, 2H, Ar–H], 7.78 [d, 2H, Ar–H], 7.78 [d, 2H, Ar–H], 8.74 [s, 1H, N=CH], 10.10 [s, 1H, Ar–OH], 11.07 [br s, 1H, CONH], 11.68 [s, 1H, Ar–OH]; ^{13}C NMR (100 MHz, DMSO): δ 11.8, 14.1, 37.0, 60.9, 71.1, 103.7,

104.7, 108.2, 108.6, 111.1, 123.1, 125.9, 127.7 (2C), 128.3 (2C), 128.6 (2C), 132.0, 132.1 (2C), 132.7, 133.8, 139.4, 142.1, 146.0, 162.2, 162.5, 165.9 and 175.5;

ethyl 5-(4-bromophenyl)-2-methyl-1-(1-oxo-3-phenyl-1-(2-(2,3,4-trihydroxybenzylidene) hydrazinyl)propan-2-yl)-1H-pyrrole-3-carboxylate (PheOH-2)

Solid; Yield 89%; Melting point 207.6 °C; IR *ν*max: 3426 cm^{-1} (O-H broad), 3268 cm^{-1} (N–H stretch), 1712 cm^{-1} (C=O stretch), 1668 cm^{-1} (C=N imine); ^{1}H NMR (δH, 400 MHz, DMSOd6): δ 1.30 [t, 3H, OCH_2CH_3], 2.47 [s, 3H, CH_3], 2.94-3.19 [m, 2H, Phe-CH_2], 4.29 [q, 2H, OCH_2CH_3], 5.02 [t, 1H, Phe-α-CH], 6.27 [d, 1H, Ar–H], 6.33 [d, 1H, Ar-H], 6.78 [s, 1H, pyrrole-H], 7.10 [d, 1H, Ar–H], 7.19 [t, 1H, Ar-H], 7.21 [t, 1H, Ar-H], 7.21 [t, 1H, Ar-H], 7.23 [t, 1H, Ar-H], 7.23 [t, 1H, Ar-H],], 7.55 [d, 2H, Ar–H], 7.55 [d, 2H, Ar–H], 7.78 [d, 2H, Ar–H], 7.78 [d, 2H, Ar–H], 8.73 [s, 1H, Ar–OH], 8.74 [s, 1H, N=CH], 9.48 [s, 1H, Ar–OH], 11.07 br [s, 1H, CONH], 13.78 [s, 1H, Ar–OH]; ^{13}C NMR (100 MHz, DMSOd6): δ 11.8, 14.1, 37.0, 60.9, 71.1, 104.7, 108.2, 110.0, 112.5, 123.1, 125.9, 126.4, 127.7 (2C), 128.3 (2C), 128.6 (2C), 132.0, 132.1 (2C), 132.7, 136.1, 139.4, 142.1, 146.0, 152.4, 153.1, 165.9 and 175.5;

ethyl 5-(4-bromophenyl)-2-methyl-1-(1-oxo-3-phenyl-1-(2-(2,4,5-trihydroxybenzylidene) hydrazinyl)propan-2-yl)-1H-pyrrole-3-carboxylate (PheOH-3)

Solid; Yield 88%; Melting point 241.2 °C; IR *ν*max: 3462 cm^{-1} (O-H broad), 3280 cm^{-1} (N–H stretch), 1718 cm^{-1} (C=O stretch), 1675 cm^{-1} (C=N imine); ^{1}H NMR (δH, 400 MHz, DMSOd6): δ 1.30 [t, 3H, OCH2CH3], 2.47 [s, 3H, CH_3], 2.94-3.19 [m, 2H, Phe-CH_2], 4.29 [q, 2H, OCH_2CH_3], 5.02 [t, 1H, Phe-α-CH], 6.15 [d, 1H, Ar-H], 6.78 [s, 1H, pyrrole-H], 6.91 [d, 1H, Ar-H], 7.19 [t, 1H, Ar-H], 7.21 [t, 1H, Ar-H], 7.21 [t, 1H, Ar-H], 7.23 [t, 1H, Ar-H], 7.23 [t, 1H, Ar-H],], 7.55 [d, 2H, Ar–H], 7.55 [d, 2H, Ar–H], 7.78 [d, 2H, Ar–H], 7.78 [d, 2H, Ar–H], 8.74 [s, 1H, N=CH], 9.48 [s, 1H, Ar–OH], 9.48 [s, 1H, Ar–OH], 11.07 [br s, 1H, CONH], 11.68 [s, 1H, Ar–OH]; ^{13}C NMR (100 MHz, DMSO): δ 11.8, 14.1, 37.0, 60.9, 71.1, 104.7, 105.1, 108.2, 112.5, 117.7, 123.1, 125.9, 127.7 (2C), 128.3 (2C), 128.6 (2C), 132.0, 132.1 (2C), 132.7, 138.7, 139.4, 142.1, 146.0, 152.4, 155.0, 165.9 and 175.5;

ethyl 5-(4-bromophenyl)-2-methyl-1-(1-oxo-3-phenyl-1-(2-(2,4,6-trihydroxybenzylidene) hydrazinyl)propan-2-yl)-1H-pyrrole-3-carboxylate (PheOH-4)

Solid; Yield 89%; Melting point 230.6 °C; IR *ν*max: 3442 cm^{-1} (O-H broad), 3265 cm^{-1} (N–H stretch), 1710 cm^{-1} (C=O stretch), 1680 cm^{-1} (C=N imine); ^{1}H NMR (δH, 400 MHz, DMSOd6): δ 1.30 [t, 3H, OCH_2CH_3], 2.47 [s, 3H, CH_3], 2.94-3.19 [m, 2H, Phe-CH_2], 4.29 [q, 2H, OCH_2CH_3], 5.02 [t, 1H, Phe-α-CH], 6.78 [s, 1H, pyrrole-H], 7.08 [d, 1H, Ar-H], 7.08 [d, 1H, Ar-H], 7.19 [t, 1H, Ar-H], 7.21 [t, 1H, Ar-H], 7.21 [t, 1H, Ar-H], 7.23 [t, 1H, Ar-H], 7.23 [t, 1H, Ar-H],], 7.55 [d, 2H, Ar–H], 7.55 [d, 2H, Ar–H], 7.78 [d, 2H, Ar–H], 7.78 [d, 2H, Ar–H], 8.39 [s, 1H, N=CH], 10.27 [s, 1H, Ar–OH], 10.27 [s, 1H, Ar–OH], 10.40 [s, 1H, Ar–OH], 11.07 [br s, 1H, CONH]; ^{13}C NMR (100 MHz, DMSOd6): δ 11.8, 14.1, 37.0, 60.9, 71.1, 96.3 (2C), 104.7, 106.2, 108.2, 123.1, 125.9, 127.7 (2C), 128.3 (2C), 128.6 (2C), 132.0, 132.1 (2C), 132.7, 139.4, 142.1, 143.3,163.6, 163.9 (2C), 165.9 and 175.5;

ethyl 5-(4-bromophenyl)-1-(1-(2-(2,4-dihydroxybenzylidene)hydrazinyl)-3-(1H-indol-3-yl)-1-oxopropan-2-yl)-2-methyl-1H-pyrrole-3-carboxylate (TrpOH-1)

Solid; Yield 83%; Melting point 203.1 °C; IR *ν*max: 3373 cm^{-1} (O-H broad), 3235 cm^{-1} (N–H stretch), 1710 cm^{-1} (C=O stretch), 1660 cm^{-1} (C=N imine); ^{1}H NMR (δH, 400 MHz, DMSOd6): δ 1.30 [t, 3H, OCH2CH3], 2.47 [s, 3H, CH_3], 2.81-3.06 [m, 2H, Tryp-CH_2], 4.29 [q, 2H, OCH_2CH_3], 5.02 [t, 1H, N–CH], 6.33 [d, 1H, Ar–H], 6.78 [s, 1H, pyrrole-H], 6.98 [d, 1H, Ar–H], 7.06 [t, 1H, Ar–H], 7.18 [t, 1H, Ar–H], 7.33 [d, 1H, Ar–H], 7.52 [d, 1H, Ar–H], 7.54 [d, 1H, Ar–H], 7.55 [d, 2H, Ar–H], 7.55 [d, 2H, Ar–H], 7.57 [d, 1H, Ar–H], 7.78 [d, 2H, Ar–H], 7.78 [d, 2H, Ar–H], 8.74 [s, 1H, CH=N], 10.10 [s, 1H, OH], 10.73 [s, 1H, indole-NH], 11.07 [br s, 1H, CONH], 11.68 [s, 1H, OH]; ^{13}C NMR (100 MHz, DMSOd6): δ 11.8, 14.1, 30.7, 60.9, 72.8, 103.7, 104.7, 108.2, 108.6, 110.8, 111.1 (2C), 118.8, 119.8, 121.7, 123.0, 123.1, 127.4, 128.3 (2C), 132.0, 132.1 (2C), 132.7, 133.8, 136.5, 142.1, 146.0, 162.2, 162.5, 165.9 and 175.5;

ethyl 1-(3-(1H-indol-3-yl)-1-oxo-1-(2-(2,3,4-trihydroxybenzylidene)hydrazinyl)propan-2-yl)-5-(4-bromophenyl)-2-methyl-1H-pyrrole-3-carboxylate (TrpOH-2)

Solid; Yield 81%; Melting point 215.2 °C; IR *ν*max: 3385 cm^{-1} (O-H broad), 3228 cm^{-1} (N–H stretch), 1708 cm^{-1} (C=O stretch), 1658 cm^{-1} (C=N imine); ^{1}H NMR (δH, 400 MHz, DMSOd6): δ 1.30 [t, 3H, OCH_2CH_3], 2.47 [s, 3H, CH_3], 2.81-3.06 [m, 2H, Tryp-CH_2], 4.29 [q, 2H, OCH_2CH_3], 5.02 [t, 1H, N–CH], 6.27 [d, 1H, Ar–H], 6.78 [s, 1H, pyrrole-H], 6.98 [d, 1H, Ar–H], 7.06 [t, 1H, Ar–H], 7.10 [d, 1H, Ar–H], 7.18 [t, 1H, Ar–H], 7.33 [d, 1H, Ar–H], 7.55 [d, 2H, Ar–H], 7.55 [d, 2H, Ar–H], 7.57 [d, 1H, Ar–H], 7.78 [d, 2H, Ar–H], 7.78 [d, 2H, Ar–H], 8.73 [s, 1H, Ar–OH], 8.74 [s, 1H, N=CH], 9.48 [s, 1H, Ar–OH], 10.73 [s, 1H, indole-NH], 11.07 [br s, 1H, CONH], 13.78 [s, 1H, Ar–OH]; ^{13}C NMR (100 MHz, DMSOd6): δ 11.8, 14.1, 30.7, 60.9, 72.8, 104.7, 108.2, 110.0, 110.8, 111.1, 112.5, 118.8, 119.8, 121.7, 123.0, 123.1, 126.4, 127.4, 128.3 (2C), 132.0, 132.1 (2C), 132.7, 136.1, 136.5, 142.1, 146.0, 152.4, , 153.1, 165.9 and 175.5;

ethyl 1-(3-(1H-indol-3-yl)-1-oxo-1-(2-(2,4,5-trihydroxybenzylidene)hydrazinyl)propan-2-yl)-5-(4-bromophenyl)-2-methyl-1H-pyrrole-3-carboxylate (TrpOH-3)

Solid; Yield 83%; Melting point 251.2 °C; IR *ν*max: 3373 cm^{-1} (O-H broad), 3245 cm^{-1} (N–H stretch), 1715 cm^{-1} (C=O stretch), 1650 cm^{-1} (C=N imine); ^{1}H

NMR (δH, 400 MHz, DMSOd6): δ 1.30 [t, 3H, OCH_2CH_3], 2.47 [s, 3H, CH_3], 2.81-3.06 [m, 2H, Tryp-CH_2], 4.29 [q, 2H, OCH_2CH_3], 5.02 [t, 1H, N–CH], 6.15 [d, 1H, Ar–H], 6.78 [s, 1H, pyrrole-H], 6.91 [d, 1H, Ar–H], 6.98 [d, 1H, Ar–H], 7.06 [t, 1H, Ar–H], 7.18 [t, 1H, Ar–H], 7.33 [d, 1H, Ar–H], 7.55 [d, 2H, Ar–H], 7.55 [d, 2H, Ar–H], 7.57 [d, 1H, Ar–H], 7.78 [d, 2H, Ar–H], 7.78 [d, 2H, Ar–H], 8.74 [s, 1H, N=CH], 9.48 [s, 1H, Ar–OH], 9.48 [s, 1H, Ar–OH], 10.73 [s, 1H, indole-NH], 11.07 [br s, 1H, CONH], 11.68 [s, 1H, OH]; ^{13}C NMR (100 MHz, DMSOd6): δ 11.8, 14.1, 30.7, 60.9, 72.8, 104.7, 105.1, 108.2, 110.8, 111.1, 112.5, 117.7, 118.8, 119.8, 121.7, 123.0, 123.1, 127.4, 128.3 (2C), 132.0, 132.1 (2C), 132.7, 136.5, 138.7, 142.1, 146.0, 152.4, 155.1, 165.9 and 175.5;

ethyl 1-(3-(1H-indol-3-yl)-1-oxo-1-(2-(2,4,6-trihydroxybenzylidene)hydrazinyl)propan-2-yl)-5-(4-bromophenyl)-2-methyl-1H-pyrrole-3-carboxylate (TrpOH-4)

Solid; Yield 85%; Melting point 216.4 °C; IR *ν*max: 3407 cm^{-1} (O-H broad), 3220 cm^{-1} (N–H stretch), 1718 cm^{-1} (C=O stretch), 1670 cm^{-1} (C=N imine); ^{1}H NMR (δH, 400 MHz, DMSOd6): δ 1.30 [t, 3H, OCH_2CH_3], 2.47 [s, 3H, CH_3], 2.81-3.06 [m, 2H, Tryp-CH_2], 4.29 [q, 2H, OCH_2CH_3], 5.02 [t, 1H, N–CH], 6.78 [s, 1H, pyrrole-H], 6.98 [d, 1H, Ar–H], 7.06 [t, 1H, Ar–H], 7.08 [d, 1H, Ar-H], 7.08 [d, 1H, Ar-H], 7.18 [t, 1H, Ar–H], 7.33 [d, 1H, Ar–H], 7.55 [d, 2H, Ar–H], 7.55 [d, 2H, Ar–H], 7.57 [d, 1H, Ar–H], 7.78 [d, 2H, Ar–H], 7.78 [d, 2H, Ar–H], 8.39 [s, 1H, N=CH], 10.27 [s, 1H, Ar–OH], 10.27 [s, 1H, Ar–OH], 10.40 [s, 1H, Ar–OH], 10.73 [s, 1H, indole-NH], 11.07 [s, 1H, CONH]; ^{13}C NMR (100 MHz, DMSOd6): δ 11.8, 14.1, 30.7, 60.9, 72.8, 96.3 (2C), 104.7, 106.2, 108.2, 110.8, , 111.1, 118.8, 119.8, 121.7, 123.0, 123.1, 127.4, 128.3 (2C), 132.0, 132.1 (2C), 132.7, 136.5, 142.1, 143.3, 163.6, 163.9 (2C), 165.9 and 175.5;

Antioxiadnt assays

DPPH radical scavenging assay

The 2,2-diphenyl-1-picrylhydrazyl (DPPH) free radical scavenging assay was conducted following the standard Brand-Williams protocol with minor modifications (Brand-Williams et al. 1995). Stock solutions of test compounds were prepared at 1 mg/mL in DMSO, and serial dilutions were made to achieve final concentrations ranging from 12.5–200 μM in the assay mixture. Fresh DPPH solution (0.1 mM in methanol) was prepared daily and 2 mL was mixed with 2 mL of each sample solution in test tubes. The mixtures were vortexed thoroughly and incubated in the dark at room temperature for 30 min to allow complete reaction. Absorbance was measured at 515 nm using a UV/Vis spectrophotometer after triplicate measurements. Methanol with DPPH served as the blank ($Abs_{control}$), DMSO/methanol as sample blank, and Trolox as the reference standard.

DPPH scavenging activity was calculated using the following equation:

$$DPPH_{scavenging\ activity} = Abs_{control} - Abs_{sample} / Abs_{control} \times 100\%$$

Where $Abs_{control}$ is the absorbance of DPPH radical in methanol and Abs_{sample} is the absorbance of DPPH radical solution mixed with sample. IC_{50} values (concentration inhibiting 50% DPPH) were determined by nonlinear regression of dose-response curves.

ABTS radical cation scavenging assay

The 2,2'-azino-bis(3-ethylbenzothiazoline-6-sulfonic acid) (ABTS) radical cation assay was performed according to Arnao et al. with optimization for hydrazone derivatives (Arnao et al. 1996). ABTS stock solution was generated by mixing equal volumes of 7 mmol/L ABTS and 2.45 mmol/L potassium persulfate, followed by incubation in the dark at room temperature for 14 h to achieve complete radical formation. The stock was diluted with phosphate buffer (pH 7.4) to obtain working solution with absorbance 0.70 ± 0.02 at 734 nm. Sample solutions (1 mg/mL in DMSO) were diluted to final assay concentrations (25–250 μM), and 1 mL was reacted with 3 mL ABTS working solution for 15 min at 25 °C in the dark. Absorbance was recorded at 734 nm in triplicate. Buffer replaced samples for blank correction, and Trolox served as positive control. Inhibition percentages were calculated using the identical formula as DPPH. IC_{50} values were interpolated from sigmoidal dose-response curves.

Molecular docking

Molecular docking studies were performed using a structure of keap1 kelch domain (ID: 4L7B) as the target. The binding pocket was identified based on the active conformation of the co-crystallized ligand. Protein structures were prepared using the Maestro Protein Preparation Wizard by adding missing hydrogens, removing non-essential water molecules, and minimizing the structure with the OPLS4 force field. The selected pyrrole-base ligand was prepared by generating dominant ionization states at physiological pH (7.4), optimizing hydrogen bonding networks and performing geometry minimization using the OPLS4 force field. Docking was conducted with Glide employing the extra precision (XP) mode. XP docking provided final binding energy calculations and interaction maps. Protein-ligand complexes were analyzed and visualized using Maestro's XP Visualizer module.

ADME studies

The physicochemical and ADME profiles of the newly synthesized pyrrole-based hydrazide-hydrazones (GlyOH1-4, BAlaOH1-4, IleOH1-4, PheOH1-4, TrpOH1-4) were predicted using the QikProp module implemented in Maestro from Schrödinger Suite (2026-1). QikProp computes approximately 40 physicochemical descriptors, octanol-water partition coefficients (logPo/w), aqueous solubility (logS), and pharmaceutically relevant properties such as human intestinal absorption, Caco-2 and cell permeabilities, logBB for brain/blood partition, and apparent permeability. These predictions were performed in

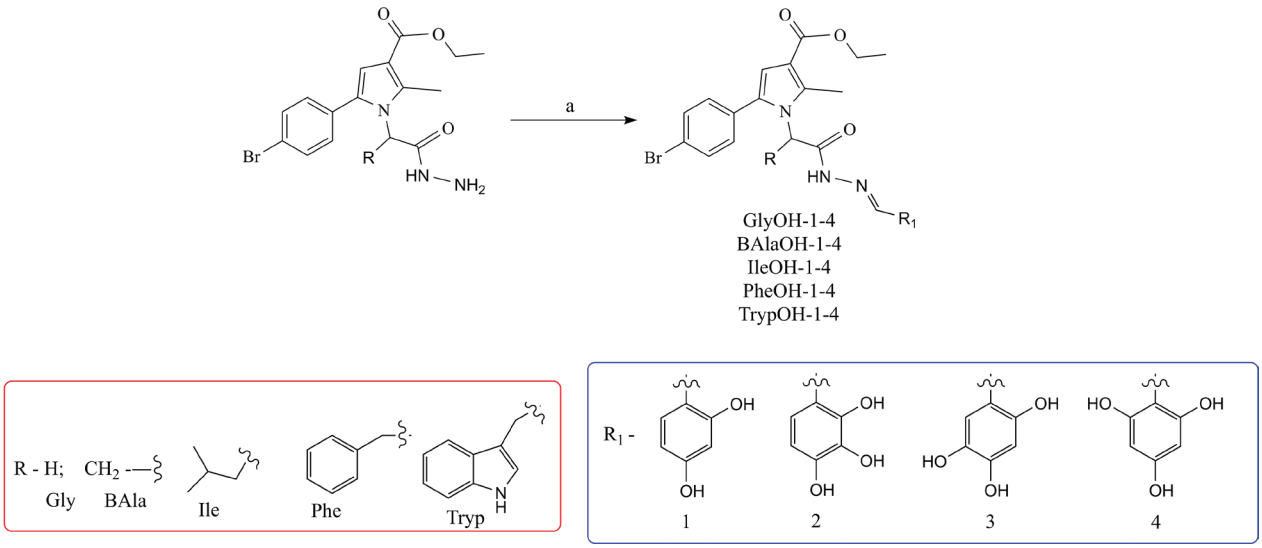

Scheme 1. General synthetic approach for the synthesis of pyrrole-based hydrazide-hydrazone derivatives (GlyOH1-4, BAlaOH1-4, IleOH1-4, PheOH1-4, TrpOH1-4).

the normal mode, which accounts for molecular flexibility without active transport contributions, using the OPLS4 force field for 3D structure preparation. The resulting drug-likeness was evaluated based on the number of property descriptors falling outside known ranges for 95% of commercially available drugs

Results and discussion

Design and synthesis

The design of the pyrrole-based hydrazide-hydrazones was rationally driven by structure-activity relationship insights from N-pyrrolyl hydrazones, which exhibit potent free radical scavenging via HAT (hydrogen atom transfer) and SET (single electron transfer) mechanisms in DPPH/ABTS assays (Lessigiarska et al. 2012). The electron-rich pyrrole ring serves as a radical-stabilizing core, while the hydrazone N-H facilitates deprotonation and resonance delocalization of the aminyl radical. The pyrrole ring acts as the main radical-trapping unit, with its electron-rich positions quickly reacting with harmful species like - OH and O_2^- (Lusardi et al. 2024). The hydrazone N-H group supports this by losing a proton to form a stable radical that spreads across the molecule. Different amino acids were chosen to improve these effects: glycine and β-alanine add flexible polar groups for water solubility and HAT in aqueous environments; isoleucine provides hydrophobic branching for better cell membrane access; phenylalanine allows π-stacking with radicals; and tryptophan uses its indole ring for extra scavenging of peroxyl radicals while potentially activating the Nrf2 pathway to boost natural antioxidants like glutathione.

The synthetic routes used to prepare the target pyrrole-based hydrazide-hydrazones, namely GlyOH1-4, BAlaOH1-4, IleOH1-4, PheOH1-4, and TrpOH1-4, from the corresponding aldehydes 1-4 are presented in Scheme 1.

The target pyrrole-based hydrazide-hydrazones were successfully synthesized via nucleophilic addition-elimination condensation of the corresponding amino acid hydrazides (derived from glycine, β-alanine, isoleucine, phenylalanine, and tryptophan) with aldehydes 1-4. Reactions proceeded quantitatively in glacial acetic acid under reflux for 1 hr, affording the products after several washings with hexane.

The spectroscopic data (IR, ^{1}H NMR, ^{13}C NMR) for the pyrrole-based hydrazide-hydrazones unequivocally confirm their targeted structures, high purity, and successful hydrazone condensation. All compounds were obtained as solids in excellent yields (83-95%) with sharp melting points (168-251 °C), indicative of stable crystalline forms suitable for biological evaluation.

The IR spectra display consistent signatures of the hydrazone pharmacophore across the series: broad O-H stretches (3322-3404 cm^{-1}) from phenolic hydroxy groups involved in intramolecular H-bonding, N-H stretches (3220-3285 cm^{-1}) for hydrazide and indole (Trp) moieties, intense C=O bands (1708-1728 cm^{-1}) from ester and amide carbonyls, and C=N imine stretches (1650-1680 cm^{-1}), validating the condensation without side reactions. Minor shifts (e.g., lower C=N in TrpOH-4 at 1670 cm^{-1}) reflect extended conjugation with the indole ring, enhancing electron delocalization for antioxidant activity.

^{1}H NMR spectra (400 MHz, DMSO-d^6) reveal diagnostic singlets for the azomethine proton (N=CH) at δ 8.39-8.74 ppm, deshielded by the imine and H-bonding, with upfield shift in 2,4,6-trihydroxy analogs (e.g., GlyOH-4 δ 8.39) due to symmetric H-bonding. Common motifs include the ethyl ester (δ 1.30 t, 3H; 4.29 q, 2H), pyrrole-CH3 (δ 2.47 s, 3H), p-bromophenyl (δ 7.55 d, 7.78 d, 4H), and phenolic OH (δ 9.48-13.78, broad s due to exchange).

The analytical and spectroscopic data of the newly synthesized compounds are in full agreement with their predicted structures and are detailed in the Materials and Methods section.

Antioxidant activity

The *in vitro* tests that were used to determine the radical-scavenging activity of the newly synthesized pyrrole-containing hydrazide-hydrazones are the ABTS test and the DPPH test. These tests are reliable, accurate, fast, and easily reproducible. Trolox, a structural analog of vitamin E, which is widely used as a standard in *in vitro* tests for antioxidant activity, was used as the standard in both tests.

ABTS assay

The ABTS test consists of the interaction of the studied compounds with the cationic radical $ABTS^{\bullet+}$. This radical has a characteristic blue color with four absorption maxima in the visible region. In the presence of antioxidant activity from the tested substance, decolorization is observed. The mechanism of radical-scavenging action in the ABTS test is electron transfer, which is why substances that are good electron donors show the highest activity using this method. Typically, the decrease in absorption at 734 nm is measured, which is an indicator of the strength of the radical-scavenging effect. The results of the conducted ABTS test on the newly synthesized compounds are presented in Table 1.

The results show that the highest ABTS radical-scavenging activity is demonstrated by the compound TrypOH-3, followed by BalaOH-3, TrypOH-4, BalaOH-2, TrypOH-2, BalaOH-1, and PheOH-2. These substances possess activity that is higher or comparable to that of the standard Trolox. The compounds LeuOH-2, PheOH-3, LeuOH-3, and GlyOH-2 also show good activity. For the remaining substances, the activity is drastically weaker.

DPPH assay

The DPPH test involves measuring the interaction between the tested compounds and the free radical 2,2-Diphenyl-1-picrylhydrazyl (DPPH). DPPH is colored violet and has an absorption maximum at 517 nm. Upon interaction with substances possessing radical-scavenging activity, it is reduced to its DPPH-H form. This reduced form does not have an absorption maximum at 517 nm. The radical-scavenging activity of the studied compounds is determined by measuring the decrease in absorption at the specified wavelength after interaction between a solution of the tested samples and a solution of DPPH. The best DPPH radical-scavenging activity is demonstrated by substances that are good proton donors because proton transfer is the main mechanism of interaction in this method. The results of the conducted DPPH test on the newly synthesized compounds are presented in Table 2.

The results indicate that, once again, the compound with the highest activity is TrypOH-3. Other substances possessing better or comparable activity to the Trolox standard are TrypOH-4, BalaOH-3, PheOH-2, BalaOH-1, TrypOH-2, and LeuOH-3. Slightly weaker activity is demonstrated by BalaOH-2, PheOH-3, and LeuOH-1. The remaining compounds have significantly lower activity, with IC_{50} values around and above 100 μM.

SAR

Structure-activity relationship (SAR) analysis of the synthesized pyrrole-containing hydrazide-hydrazone derivatives revealed consistent trends in radical-scavenging

Table 1. IC_{50} values of ABTS radical-scavenging activity of the studied substances.

Compound	IC_{50} (μM ± SD)
GlyOH-1	197.26 ± 0.40
GlyOH-2	32.56 ± 0.27
GlyOH-3	467.23 ± 0.32
GlyOH-4	201.78 ± 0.18
BAlaOH-1	18.23 ± 0.10
BAlaOH-2	12.12 ± 0.16
BAlaOH-3	7.23 ± 0.24
BAlaOH-4	>1000
LeuOH-1	98.24 ± 0.30
LeuOH-2	24.01 ± 0.28
LeuOH-3	30.42 ± 0.48
LeuOH-4	224.56 ± 0.62
PheOH-1	374.53 ± 0.32
PheOH-2	20.84 ± 0.32
PheOH-3	28.54 ± 0.16
PheOH-4	498.23 ± 0.50
TrypOH-1	174.28 ± 0.67
TrypOH-2	15.32 ± 0.30
TrypOH-3	3.96 ± 0.20
TrypOH-4	9.92 ± 0.42
Trolox	17.04 ± 0.26

Table 2. IC_{50} values of DPPH radical-scavenging activity of the studied substances.

Compound	IC_{50} (μM ± SD)
GlyOH-1	299.63 ± 0.63
GlyOH-2	323.46 ± 0.46
GlyOH-3	399.96 ± 0.27
GlyOH-4	213.88 ± 0.54
BAlaOH-1	28.96 ± 0.24
BAlaOH-2	46.24 ± 0.48
BAlaOH-3	22.13 ± 0.10
BAlaOH-4	>1000
LeuOH-1	62.01 ± 0.32
LeuOH-2	93.56 ± 0.28
LeuOH-3	36.03 ± 0.52
LeuOH-4	>1000
PheOH-1	423.01 ± 0.64
PheOH-2	28.92 ± 0.08
PheOH-3	49.53 ± 0.46
PheOH-4	>1000
TrypOH-1	331.52 ± 0.29
TrypOH-2	30.94 ± 0.23
TrypOH-3	9.17 ± 0.09
TrypOH-4	14.54 ± 0.14
Trolox	31.92 ± 0.12

activity across both ABTS and DPPH assays. The *in vitro* results indicate that compounds incorporating tryptophan and β-alanine fragments exhibit the highest antioxidant activity. This observation is consistent with previously reported data on the intrinsic antioxidant properties of amino acids, where tryptophan and alanine display superior activity compared to phenylalanine, leucine, and glycine (Xu et al. 2017). In agreement with this trend, the tryptophan-derived series (TrypOH) showed the most pronounced activity, with TrypOH-3 emerging as the most potent compound (IC_{50} = 3.96 μM in ABTS and 9.17 μM in DPPH), surpassing the reference standard Trolox. The enhanced activity of these derivatives can be attributed to the indole ring, which facilitates effective stabilization of radical intermediates and promotes both electron and proton transfer mechanisms.

The β-alanine derivatives (BAlaOH series) ranked second in activity, with BAlaOH-3 demonstrating significant potency (IC_{50} = 7.23 μM in ABTS and 22.13 μM in DPPH). This effect may be associated with the increased conformational flexibility and optimal spacer length of the β-alanine moiety, which likely improves the accessibility of the hydrazone functional group to reactive species. In contrast, glycine-based derivatives (GlyOH series) exhibited the weakest activity (IC_{50} values generally > 200 μM), indicating that the absence of a side chain is unfavorable for radical scavenging. Leucine (LeuOH) and phenylalanine (PheOH) derivatives showed moderate and variable activity, suggesting that bulkier aliphatic and aromatic substituents do not consistently enhance antioxidant potential.

In addition to the amino acid fragment, the nature of the aldehyde used in the azomethine condensation significantly influenced antioxidant activity. Compounds derived from 2,4,5-trihydroxybenzaldehyde and 2,3,4-trihydroxybenzaldehyde exhibited the highest radical-scavenging capacity, whereas derivatives of 2,4,6-trihydroxybenzaldehyde and 2,4-dihydroxybenzaldehyde showed comparatively lower activity. This trend suggests that the presence of two adjacent hydroxyl groups (catechol-like arrangement) markedly enhances antioxidant efficiency, likely by facilitating resonance stabilization and improving hydrogen atom donation, whereas meta-oriented hydroxyl groups are less effective.

Notably, TrypOH-3, TrypOH-4, and BAlaOH-3 were identified as dual-activity leads, outperforming Trolox in both assays. Overall, the results indicate that optimal radical-scavenging activity is achieved through a combination of an electron-rich amino acid scaffold, particularly tryptophan, and a catechol-type aromatic aldehyde moiety.

Molecular docking

Considering the established role of potent Keap1-Nrf2 disruptors as promising antioxidants and Nrf2 activators in mitigating oxidative stress-related pathologies, we selected the most active radical-scavenging ligand from our series, compound TrypOH-3, for further evaluation of its Nrf2 activation potential (Fig. 1).

TrypOH-3 exhibits a docking score of -6.25 kcal/mol, indicating moderate yet competitive affinity within the central cavity of the Keap1 Kelch domain. The binding mode is stabilized by a well-defined hydrogen-bonding network that anchors the polyhydroxylated scaffold within the polar pocket. Specifically, the phenolic OH forms a stable direct hydrogen bond with Ser602, alongside a water-mediated hydrogen bond with Ser363, reinforcing ligand positioning within the binding cleft. In addition, the indole NH participates in a hydrogen bond with Tyr525, further contributing to the stabilization of the ligand-protein complex.

A halogen-mediated interaction is also observed, where the bromine substituent engages in a directional interaction with Tyr334, consistent with halogen bonding or electrostatic stabilization. This interaction likely enhances binding specificity and contributes to the overall affinity by complementing the polar interaction network.

Collectively, these interactions suggest that TrypOH-3 effectively mimics key contacts within the Keap1-Nrf2 interface, combining hydrogen bonding, water-bridged stabilization, and halogen interactions. This multifaceted binding profile supports its potential as a non-covalent Keap1 inhibitor scaffold, with scope for further optimization to improve binding strength and selectivity.

ADME

An important aspect of characterizing the pharmacological profile of a given molecule is determining its pharmacokinetics. For this reason, for the compound showing the highest antioxidant activity – TrypOH-3, the main physicochemical parameters, which are key to pharmacokinetic behavior, were calculated *in silico*. The results are presented in Table 3.

From the predicted values, it can be seen that the compound TrypOH-3 violates Lipinski's rule in only one parameter - molecular weight. It is precisely the high molecular weight, as well as the presence of three free polar hydroxyl groups in the structure, that causes difficult passage through biological membranes, which accounts for the low absorption rate upon oral administration, as well as the reduced permeability through the blood-brain barrier. This is a potential problem when aiming for action on the central nervous

Table 3. Basic physicochemical parameters of the compound **TrypOH-3** with reference ranges.

Compound	MW	HBD	HBA	$LogP_{o/w}$	LogS	LogBB	HOA	Ro5	Metab
TrypOH-3	645.50	5	7	4.65	−7.20	−3.69	56%	1	2

MW: molecular weight (Range from 130.0 to 725.0); HBD: hydrogen bond donors (Range from 0.0 to 6.0); HBA: hydrogen bond acceptors (Range from 2.0 to 20.0); $LogP_{o/w}$: octanol/water partition coefficient (Range: from −2.0 to 6.5); LogS: Predicted aqueous solubility (Range from −6.5 to −0.5); LogBB: Predicted brain/blood partition coefficient (Range from −3.0 to 1.2); HOA: percent human oral absorption; Ro5: number of violations of Lipinski's rule of five (Range: maximum is 4); Metab: number of likely metabolic reaction.

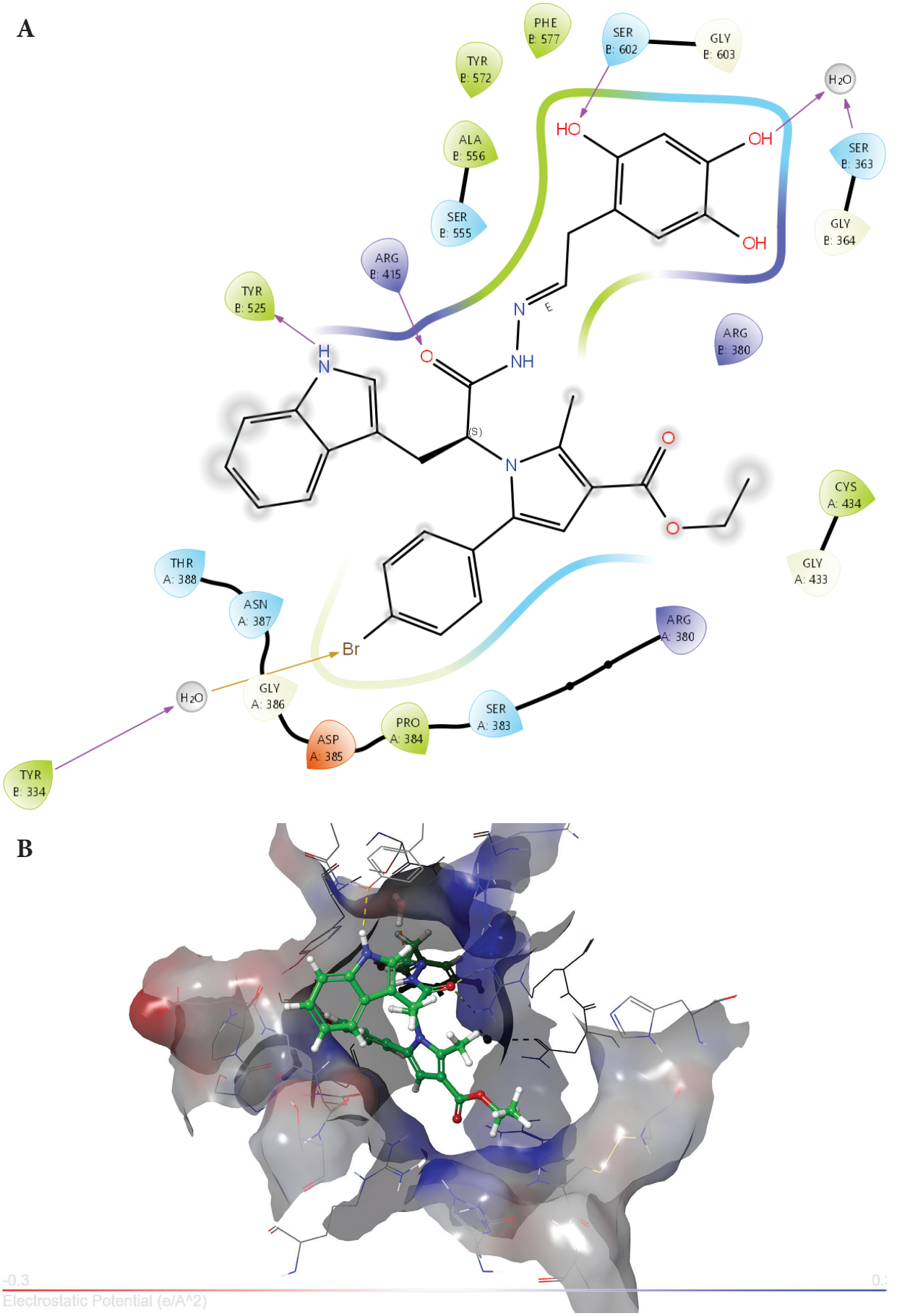

Figure 1. Molecular interactions of compound TrypOH-3 with the Keap1 Kelch domain (PDB ID: 4L7B). The pyrrole-based ligand is shown as red, blue, and green ribbons, while the active-site cavity is represented as a transparent mesh colored by electrostatic potential.

system. Creating structures with optimal pharmacokinetics is a good prospect for future scientific developments.

Conlcusion

This study successfully delivered a focused library of 20 hydroxyl-derived pyrrole hydrazide-hydrazones with potent, dual DPPH/ABTS scavenging, led by TrpOH-3's superior activity over Trolox. SAR trends underscore tryptophan's indole for radical delocalization and ortho/para-dihydroxy patterns for efficient H-atom donation, validated by docking insights into Keap1 disruption (-6.25 kcal/mol binding). Despite favorable drug-like properties, ADME profiles highlight opportunities to reduce MW for better permeability. TrpOH-3 represents a versatile lead for Nrf2-activating antioxidants targeting neurodegeneration and inflammation. Future efforts will pursue structural analogs, *in vivo* validation, and enzyme inhibition assays.

Additional information

Conflict of interest

The authors have declared that no competing interests exist.

Ethical statements

The authors declared that no clinical trials were used in the present study.

The authors declared that no experiments on humans or human tissues were performed for the present study.

The authors declared that no informed consent was obtained from the humans, donors or donors' representatives participating in the study.

The authors declared that no experiments on animals were performed for the present study.

The authors declared that no commercially available immortalised human and animal cell lines were used in the present study.

Artificial Intelligence (AI) use

The authors accept full responsibility for the content of the manuscript, including the disclosure of any use of AI.
No AI tools were used in the preparation of this manuscript.

Funding

This study was financed by the European Union-NextGenerationEU, through the National Recovery and Resilience Plan of the Republic of Bulgaria, project № BG-RRP-2.004-0004-C01.

Author contributions

All authors have contributed equally.

Author ORCIDs

Emilio Mateev https://orcid.org/0000-0002-5885-7213
Ali Irfan https://orcid.org/0000-0002-8977-3303
Stefan Kostov https://orcid.org/0009-0001-4272-3579
Alexander Zlatkov https://orcid.org/0000-0002-1695-8454

Data availability

All of the data that support the findings of this study are available in the main text.

References

Abdullah SK, See-Too WS, Mohd Mohidin TB, Mohan G (2026) Neuroinflammation as a central mechanism in Alzheimer's disease: Therapeutic insights from Schiff base derivatives. Molecules 31(3): 465. https://doi.org/10.3390/molecules31030465

Arnao MB, Cano A, Hernández-Ruiz J, García-Cánovas F, Acosta M (1996) Inhibition by L-ascorbic acid and other antioxidants of the 2.2'-azino-bis(3-ethylbenzthiazoline-6-sulfonic acid) oxidation catalyzed by peroxidase: a new approach for determining total antioxidant status of foods. Analytical Biochemistry 236(2): 255–261. https://doi.org/10.1006/abio.1996.0164

Brand-Williams W, Cuvelier ME, Berset C (1995) Use of a free radical method to evaluate antioxidant activity. LWT - Food Science and Technology 28(1): 25–30. https://doi.org/10.1016/s0023-6438(95)80008-5

Korovesis D, Rubio-Tomás T, Tavernarakis N (2023) Oxidative stress in age-related neurodegenerative diseases: An overview of recent tools and findings. Antioxidants 12(1): 131. https://doi.org/10.3390/antiox12010131

Kowalczyk P, Sulejczak D, Kleczkowska P, Bukowska-Ośko I, Kucia M, Popiel M, Wietrak E, Kramkowski K, Wrzosek K, Kaczyńska K (2021) Mitochondrial oxidative stress-A causative factor and therapeutic target in many diseases. International Journal of Molecular Sciences 22(24): 13384. https://doi.org/10.3390/ijms222413384

Lessigiarska I, Pajeva I, Prodanova P, Georgieva M, Bijev A (2012) Structure-activity relationships of pyrrole hydrazones as new anti-tuberculosis agents. Medicinal Chemistry 8(3): 462–473. https://doi.org/10.2174/1573406411208030462

Leyane TS, Jere SW, Houreld NN (2022) Oxidative stress in ageing and chronic degenerative pathologies: Molecular mechanisms involved in counteracting oxidative stress and chronic inflammation. International Journal of Molecular Sciences 23(13): 7273. https://doi.org/10.3390/ijms23137273

Lusardi M, Signorello MG, Russo E, Caviglia D, Ponassi M, Iervasi E, Rosano C, Brullo C, Spallarossa A (2024) Structure–activity relationship studies on highly functionalized pyrazole hydrazones and amides as antiproliferative and antioxidant agents. International Journal of Molecular Sciences 25(9): 4607. https://doi.org/10.3390/ijms25094607

Nakai K, Tsuruta D (2021) What are reactive oxygen species, free radicals, and oxidative stress in skin diseases? International Journal of Molecular Sciences 22(19): 10799. https://doi.org/10.3390/ijms221910799

Rana MS, Rayhan NMA, Emon MSH, Islam MT, Rathry K, Hasan MM, Islam Mansur MM, Srijon BC, Islam MS, Ray A, Rakib MA, Islam A, Kudrat-E-Zahan M, Hossen MF, Asraf MA (2024) Antioxidant activity of Schiff base ligands using the DPPH scavenging assay: An updated review. RSC Advances 14(45): 33094–33123. https://doi.org/10.1039/d4ra04375h

Xu N, Chen G, Liu H (2017) Antioxidative categorization of twenty amino acids based on experimental evaluation. Molecules 22: 2066. https://doi.org/10.3390/molecules22122066